Identification and quantification of losses in a LPT cascade by POD applied to LES data

D. Lengani1 davide.lengani@edu.unige.it, D. Simoni1, R. Pichler2, R.D. Sandberg2, V. Michelassi3 andF. Bertini4

1 DIME - Universitá di Genova, Italy 2 University of Melbourne, Melbourne, Australia 3 GE Oil & Gas S.r.l. Firenze, Italy 4GE AvioAero S.r.l., Torino, Italy

(Received 9 March 2017)

A POD based procedure has been developed to identify and account for the different contributions to the entropy production rate affecting the unsteady aerodynamic of a LP turbine blade. LES data of the extensively studied T106A cascade have been used to clearly highlight the capability of POD in identify incoming wake migration related modes, boundary layer events and coherent structures originated by the wake-boundary layer interaction process. The POD modes computed by a kinematic kernel generate a full and complete basis, where both the velocity and the enthalpy fields have been projected through an extended like POD procedure to obtain the relative coefficients. This allows to separately compute orthogonal sets of contribution to turbulent kinetic energy production, enthalpy-velocity correlation and turbulent dissipation of resolved structures, thus clearly identify the dominating modes (i.e. phenomena) responsible for the overall entropy production rate. Moreover, low order truncation of these different contributions have been grouped in two different parts: those arising from deterministic incoming wake from those due to boundary layer related events. The spatial integration of these low order truncations restricted to the time-mean boundary layer, wake mixing and the potential flow regions of the blade passage gives the opportunity of providing further information on the unsteady loss generation mechanisms, and where they mainly act. Particularly, results into the paper show that the procedure is clearly able to split losses, thus providing a new tool for a rapid and clear recognition of the different sources of losses in complex unsteady flow fields.

1. Introduction

The development of the flow field in turbine and compressor rows of multistage turbomachines is a complex three dimensional and unsteady phenomenon. The wakes shed from upstream blades induce periodic (deterministic) and stochastic oscillations at the entrance of the downstream rows, while the potential field induces strong time-varying flow distortion, making the propagation of turbulent quantities carried by upstream wakes strongly inhomogeneous and spatially dependent. During migration the upstream wake diffuses in the downstream passage, thus giving rise of turbulent and viscous losses due to superposition of different phenomena whose recognition and quantification of contribution to losses is still an hard task (van de Wall *et al.* 2000; Praisner *et al.* 2006).

In the last years detailed high fidelity computations and accurate experiments (see Wu *et al.* 2001; Michelassi *et al.* 2003; Stieger & Hodson 2005; Hodson & Howell 2005 for example) have given deep details on the unsteady wake migration process. Approaching the downstream cascade, the planar-like (2-D like) structure of the incoming wake undergoes strong bowing, tilting, dilatation and stretching processes, and it finally becomes fragmented in segments as a consequence of the relative motion between the stator and

rotor rows (Binder *et al.* 1985, 1989).

The Direct Numerical Simulation (DNS) of Wu *et al.* (2001) described in detail the stretching, dilatation and compression processes of wake filaments evolving in a LP turbine passage through a strain rate tensor principal axes analysis. They clearly showed that the wake filament developing close to the pressure side is almost aligned with the stretching direction, while on the other hand the wake centerline at the bow apex is mainly aligned with the compression direction. Moreover, as also shown in Michelassi *et al.* (2003), the largest eigenvalues are localized on the suction side of the channel, where the strongest reorientation of the jet-like structure takes place. The eigenvalue and eigenvector decomposition of the shear and strain tensors reported in Michelassi & Wissink (2015) shows that the largest (compression related) strain eigenvalues dominate the turbulent kinetic energy production due to wake migration, with a maximum in the flow region where stress and strain principal axes are almost aligned. All these observations well agree with Rogers (2002) that discusses the effects of different strain magnitudes and orientations on the turbulence produced in a planar wake. He clearly highlights that the condition with the wake patch aligned with the compression direction represents the most influencing for turbulence production, similar to what happens in the bow apex of the wake migrating in LPT passage (see also Stieger & Hodson 2005).

The incoming wakes ares also responsible for transporting the finer structures embedded in the bulk of the wake within the suction side boundary layer, thus further contributing to the excitation of the transition process (see Wu *et al.* 1999; Lengani *et al.* 2016*a*). The isocontour surfaces of the λ_2 criterion and instantaneous flow vorticity reported in Zaki *et al.* (2009) and Sarkar & Voke (2006) give a clear view of the finer structures carried by the wakes. These structures are responsible for the generation of a dense population of streaky structures in the footprint of the region perturbed by wakes, as observed either numerically and experimentally (Wu *et al.* 1999; Nagabhushana Rao *et al.* 2013; Coull & Hodson 2011; Lengani *et al.* 2016*a*). Moreover, for highly loaded turbine blades the boundary layer growing between successive wakes may undergo an intermittent separation (depending on the loading and diffusion level (Satta *et al.* 2014)), that evidently imposes an inviscid like type instability (Sarkar & Voke 2006; Simoni *et al.* 2013). In this case large scale coherent structures are shed as a consequence of the separated shear layer rollup during wake-boundary layer interaction, with dynamics similar to those characterizing the separated flow transition mechanisms observed in the steady inflow case (Alam & Sandham 2000; Jones *et al.* 2008), for example.

Overall, the unsteady aerodynamics of a LP passage is the result of the superposition of different phenomena acting in the different parts of the passage with different length and spatial scales. Each of them differently affects the loss (i.e. entropy) production mechanisms in the whole downstream passage (i.e. inside and outside the blade boundary layers) that up to now are evaluated as a whole. The possibility to split and detect the different sources of losses represents one of the main engineering goals for the advancement of efficiency of modern new generation LPT blades. Optimization procedures aimed at selectively reducing losses could be easily and effectively implemented observing the effects of design parameters on the different loss sources, instead of that on the overall. Particularly, losses due to wake diffusion in the downstream passage should be identified and isolated with respect to those being generated as a consequence of the wake boundary layer interaction. Due to the aforementioned (turbulent) stress-strain interaction mechanisms, wake migration in the potential flow region of the downstream passage gives rise to deterministic stress production, following the terminology reported in van de Wall *et al.* (2000), that can contribute a significant portion of energy degradation. The identification of this additional loss source should also be important for correcting RANS predictions

of multistage machines based on mixing plane numerical schemes, since the incoming wake turbulent content is "mixed" and seen by the downstream passage as increased homogeneous free-stream turbulence (i.e. the wake shear-stress interaction process producing losses is not resolved). Michelassi *et al.* (2015, 2016) used DNS to show that losses due to wake migration represent a non-negligible contribution of the overall losses. The different source of losses have been quantified by a control volume method (following Denton 1993) and not directly quantified from the dataset due to the difficulty in splitting boundary layer from wake migration related events. Nor phase-averaged (Hussain & Reynolds 1970) neither generalized phase-averaged methods (Bourgeois *et al.* 2013) can reach the target, since all phenomena not directly locked with the passing wake forcing are smeared out by the averaging operation and cannot be directly resolved.

Among different data analysis approach, the Proper Orthogonal Decomposition (POD) is nowadays a consolidate approach (since Lumley 1967) able to identify the different dynamics driving complex turbulent flows (e.g. Liu *et al.* 2001; van Oudheusden *et al.* 2005; Perrin *et al.* 2007; Kurelek *et al.* 2016). However, it has been rarely applied for the analysis of turbine blades perturbed by unsteady wakes. For example, in the work of Sarkar (2008), POD was applied to LES data describing the unsteady flow field of the T106 turbine cascade with Re=160000, f^+=0.68. Here, the authors pay attention to the dynamics through which the incoming wakes interact with the separated shear layer growing between wakes. While in Lengani *et al.* (2016*a*), POD has been applied to experimental data in order to discuss the flow physics of the transition induced by the periodic passing wakes. It has been shown that POD can be used to identify the large scale structures of the passing wake, as well as observing the effect of the turbulence carried by the wake on the boundary layer.

In the present paper POD has been applied to high fidelity Large Eddy Simulation (LES) of the T106 LPT cascade perturbed by traveling wakes with the aim of identifying and separately account for the different sources of unsteady losses. Particularly, a new POD based procedure is proposed for identifying and characterizing the different dynamics producing losses, analyzing their contribution to the entropy rate of change. The bi-orthonormality condition of the POD modes and related temporal coefficients is considered to compute the contribution of the individual modes' dynamics to the Reynolds stresses. An extended POD projection (Borée 2003) on the kinematic basis also provide scalar-velocity correlation terms and dissipation to heat, thus the possibilities to account for single mode contribution to the entropy rate of change. Losses generated in the boundary layer region as a consequence of streaky structures and wake-boundary layer interaction mechanisms are clearly captured and separated from losses due to wake migration and distortion in the potential flow region.

The paper is organized as follows: in § 2 the numerical method, the geometrical configuration and the flow parameters are described in detail; in § 3 the basic equations and the decomposition procedure for the moment statistics are presented; in § 4 results from POD of the LES data are described in order to clearly identify the different dynamics acting in the different parts of the LP turbine passage; once recognized, in § 5 a limited number of POD modes has been used for the identification of the contributions to the entropy rate of change due to wake migration and boundary layer related processes. Finally, in § 6 spatial integration of the different parts of the channel allows a quantitative analysis of the different regions and source of entropy rate of change.

FIGURE 1. Scheme of the computational domain and integration areas.

2. Large Eddy Simulations

The low-pressure turbine data analyzed in this paper was obtained by performing large eddy simulations (LES) using the in-house compressible multi-block structured Navier–Stokes solver HiPSTAR. A comprehensive description of its numerical methods and performance for turbomachinery applications is given in **?** and here only a brief summary of the key features is presented. The DNS were conducted using fourth-order accurate wavenumber optimized compact finite differences (**?**) in the axial/pitchwise plane and a pseudo-spectral approach, using the FFTW library, in the homogeneous spanwise direction. For the advancement in time an ultra-low storage five-step explicit fourth-order Runge–Kutta method was used (**?**). To increase the robustness of the numerical scheme and to avoid aliasing errors of the cubically nonlinear convective terms within the discretized Navier-Stokes equations, a skew-symmetric splitting of the nonlinear terms according to **?** was employed.

The code has been thoroughly tested on a range of canonical flows, such as turbulent pipes and sub- and supersonic instability waves, and has been shown to accurately

represent the flow in linear low-pressure turbine cascades (**?**), and, more recently, high-pressure turbine cascades (**?**). More recently, LES models have been implemented into the code to reduce computational cost and allow for parametric studies of turbine flows, and the suitability and accuracy of the WALE model (**?**) was demonstrated in another LPT study that investigated the concerted action of reduced frequency and flow coefficient on unsteady loss generation (Michelassi *et al.* 2016). The numerical set-up for the low-pressure turbine cases conducted to provide data for the POD analysis follows that described in Michelassi *et al.* (2015). A linear low-pressure turbine cascade using the T106A profile was considered at the isentropic conditions $Re_{2is} = 60,000$ and $M_{2is} = 0.4$, based on axial chord and isentropic exit velocity V_{2is}. The grid topology comprised four blocks for an O-type grid around the blade to ensure optimal grid quality in the vicinity of the wall, and five blocks for an H-type grid allowing for pitchwise periodicity. To ensure high-quality solutions at the block interfaces despite metric discontinuities, all blocks were connected to each other using characteristic interface conditions. At the wall a no-slip isothermal boundary condition was used. To generate periodically incoming bar wakes, an immersed boundary method was used, placing cylinder bars with diameter $D/C_{ax} = 0.02$ at $x/C_{ax} = -0.7$, moving in the pitchwise direction with velocity V_{bar}. By varying the bar spacing and/or V_{bar} the reduced frequency, $F_{red} = \frac{f \cdot C_{ax}}{V_{2is}}$, could be varied, where f is the bar passing frequency. The data analysed in this paper were obtained with $V_{bar} = -0.41 U_\infty$, where U_∞ is the incoming freestream velocity, resulting in $F_{red} = 0.61$. The simulation was initially run for 5 flow through times in 2D, then 3D simulations were restarted from the fully developed 2D result. After about 10 additional flow through times, to avoid the transient period, snapshots were collected for 20 bar passing periods for the present POD analysis.

3. Fundamental equations

The different terms involved in the entropy rate of change are first briefly introduced in order to be able then to focus on the interesting quantities to be decomposed in the following sections. Following Gibbs' equation, for a 3-D non stationary flow the entropy variation can be expressed as:

$$T_t \frac{Ds}{Dt} = \frac{Dh_t}{Dt} - \frac{1}{\rho_t} \frac{Dp_t}{Dt} \ . \tag{3.1}$$

Since the aerodynamic efficiency of LPT blades is definitively described by the mean entropy flux variation, we are interested in long time averaged quantities. Balance equations for the time-mean total enthalpy and total pressure provide the terms on the right hand side:

$$\frac{D\bar{h}_t}{Dt} = \underbrace{-\frac{\partial \overline{u_i' h_t'}}{\partial x_i}}_{I} + \underbrace{\frac{1}{Re_\infty} \overline{\sigma_{i,j} \frac{\partial u_i'}{\partial x_j}}}_{II} + Diffusive \quad Terms \ , \tag{3.2}$$

$$\frac{D\bar{p}_t}{Dt} = \underbrace{\rho \overline{u_i' u_j'} \frac{\partial \overline{u_i}}{\partial x_j}}_{III} - \underbrace{\frac{\rho}{Re_\infty} \left(\frac{\partial \overline{u_i}}{\partial x_j} \right)^2}_{IV} + Diffusive \quad Terms \ . \tag{3.3}$$

Substituting eqs. 3.2 and 3.3 in eq. 3.1 and applying it to a finite control volume of fluid elements covering one entire cascade pitch, the following balance equation can be

obtained after some algebra:

$$\tilde{s}_2 - \tilde{s}_1 = \frac{1}{\dot{m}} \left(\int_V \frac{(I+II)}{T_t} dV - \int_V \frac{(III+IV)}{T_t \rho_t} dV \right) , \tag{3.4}$$

where $\tilde{s}_i$ denotes the mass-averaged inlet and outlet cascade entropy per unit mass. The first term on the right hand side provides the entropy rate of change due to the enthalpy-velocity correlation terms (i.e. the vector of the scalar stresses) and the fine (resolved) turbulent scales dissipation producing heat. The contribution due to mechanical energy dissipation comes from the second term on the right and side. Here viscous and turbulent stresses produce entropy. All the other diffusive-like terms appearing in Eqs.3.2 and 3.3 do not contribute to the balance described by Eq. 3.4, since their spatial integral values are identically zero. Moreover, contributions due to the unresolved scales will contribute to the balance, especially due to dissipation. However, in the present LES results they only account for a percentage smaller than 5% of the overall TKE, and only minor inaccuracies in the quantitative estimation reported into the last section of the paper are expected.

3.1. *Data processing*

In the present work, all fluctuating quantities are decomposed in order to separate the different dynamics and analyze their contribution to the rate of change of entropy. POD of the flow field is chosen as a suitable tool for such a loss split. With the kernel of the POD defined with the instantaneous velocity snapshots (see Sirovich 1987) the POD provides a triplet of information: the eigenvalues $\lambda^{(k)}$, the eigenvectors $\chi^{(k)}$ and the POD modes $\phi^{(k)}$. The eigenvalue of the k^{th} mode represents the energy contribution of the mode to the total kinetic energy of velocity fluctuations. The eigenvectors constitute an orthogonal basis and retain the temporal information related to each mode. The POD modes constitute an orthogonal basis that provides the spatial information identifying coherent structures in the flow.

The terms I, II and III of equation 3.4, involved in the entropy rate of change, are due to the turbulence activity, being defined by fluctuating quantities. The contribution per POD mode of each of these terms can be efficiently computed exploiting the properties of POD. Particularly, since the POD modes and eigenvectors are orthogonal, the Reynolds shear and normal stresses can be computed as follows:

$$\overline{u_i' u_j'} = \sum_k \lambda^{(k)} \phi_{u_i}^{(k)} \phi_{u_j}^{(k)} . \tag{3.5}$$

The term $\lambda^{(k)} \phi_{u_i}^{(k)} \phi_{u_j}^{(k)}$ represents the contribution of the k^{th} POD mode to the overall time-mean Reynolds stresses. This property of POD can be applied to determine the individual modes' contribution to the TKE production (the term III in Eq. 3.4) with reversed sign, that can be generically represented (using index i, j) as p_{ij}:

$$p_{ij} = -\overline{u_i' u_j'} \frac{\partial \overline{u}_i}{\partial x_j} . \tag{3.6}$$

Substituting Eqs. 3.5 into Eq. 3.6, the contribution of each POD mode to the TKE production rate p_{ij} can be written as:

$$p_{ij}^{(k)} = -\lambda^{(k)} \phi_{u_i}^{(k)} \phi_{u_j}^{(k)} \frac{\partial \overline{u}_i}{\partial x_j}, \quad with \quad p_{ij} = \sum_k p_{ij}^{(k)} . \tag{3.7}$$

As shown previously in Lengani *et al.* (2016*b*), a combination of POD modes of the velocity field and their spatial derivatives can be used to obtain the dissipation of energy

due to the resolved scales (the term II into Eq. 3.4). It is expressed as:

$$\frac{1}{Re_\infty}\overline{\sigma_{i,j}\frac{\partial u_i'}{\partial x_j}} = \frac{1}{Re_\infty}\left(\frac{\partial \phi_i^{(k)}}{\partial x_j} + \frac{\partial \phi_j^{(k)}}{\partial x_i}\right)\frac{\partial \phi_j^{(k)}}{\partial x_i} \ . \tag{3.8}$$

The enthalpy-velocity correlation term (term I of Eq. 3.4) can be expressed as:

$$-\frac{\partial \overline{u_i' h_t'}}{\partial x_i} = -\sum_k \frac{\partial \phi_{u_i}^{(k)} \phi_{h_t}^{(k)}}{\partial x_i} \ , \tag{3.9}$$

where the k^{th} POD mode of the enthalpy $\phi_{h_t}^{(k)}$ is obtained by projecting the instantaneous enthalpy fields h_t' onto the orthonormal basis spanned by the kinetic POD eigenvector ($\chi^{(k)}$) of the velocity correlation tensor, like the extended POD procedure proposed by Borée (2003):

$$\phi_{h_t}^{(k)} = \sum_{n=1}^{N} \chi_n^{(k)} h_{tn} \ . \tag{3.10}$$

where n is the discrete time interval. According to these equations, each POD mode contributes a part of the total entropy generation, which can be analyzed separately in order to identify the role it plays in the different dynamics affecting the unsteady flow field of the LPT cascade. While term IV of Eq. 3.4 is the viscous dissipation due to the mean flow distortion that accounts for a large quota of the overall losses (about 40%).It is concentrated on the boundary layer and profile wake mixing regions, as expected, with negligible contribution into the potential flow region of the blade passage affected by incoming wake migration. Since this term is not dependent on the dynamics and cannot be decomposed, it will no further discussed in the following but only account for in the cumulative distributions reported at the end of the paper.

4. Results

4.1. *Instantaneous Flow Structures*

The instantaneous flow field of the LES is depicted in Fig. 2 for two typical snapshots within a wake passing cycle in order to give a qualitative view of the fluctuating field and its complexity. The flow field is viewed at the mid-span section of the simulation and is represented with vectors of the fluctuating velocity and iso-contours of the fluctuating pressure (i.e. velocity and pressure are decomposed with the Reynolds' decomposition, subtracting the mean value). In the first frame the instantaneous velocity vectors point, in the mid-section of the passage, towards the suction side of the bottom blade. They unveil the remnants of the wake "centerline" and this flow region is evidently characterized by negative relative pressure (blue area in the plot). Disordered motion can also be recognized in the surrounding of the blade leading edge, as well as in the rear part of the blade suction side. At the leading edge the pressure field shows localized spots at elevated pressure. The successive frame, where the wake centerline is leaving the simulation domain, shows a complex pattern in both the potential flow region and in the proximity of the wall. Now the instantaneous velocity vectors point away from the suction side wall at around 0.5 of axial chord downstream of the leading edge, and locally the pressure increases. At this time instant the structures carried by the upstream wake towards the suction side boundary layer are interacting with the rear part of the blade.

The structures originating during this interaction are highly three dimensional as

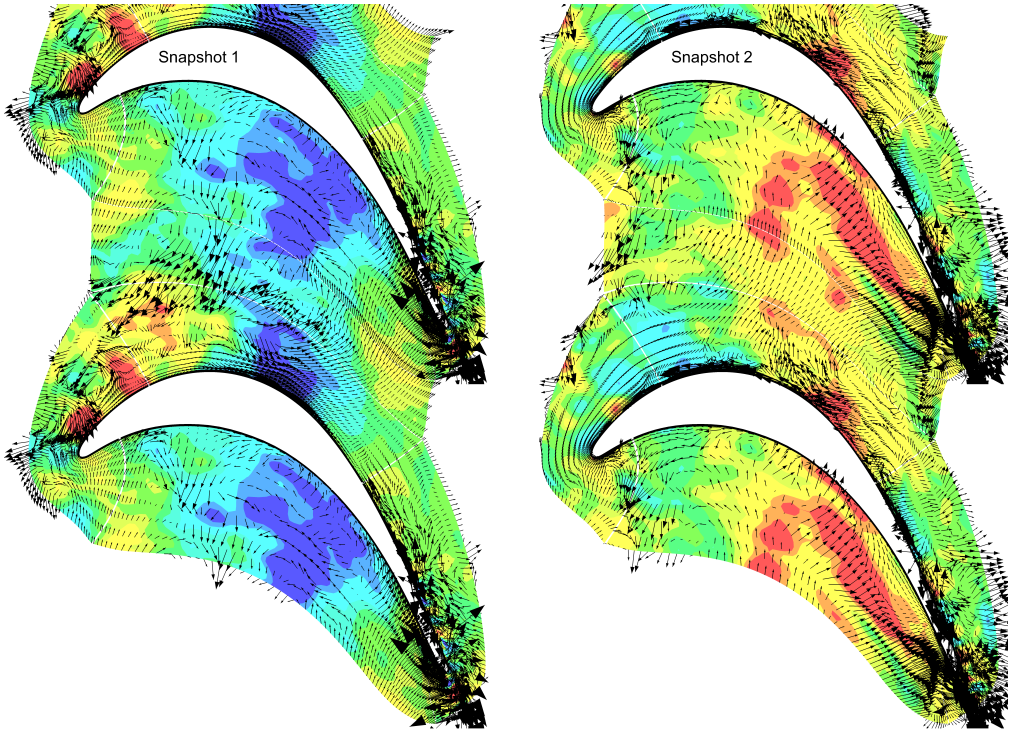

FIGURE 2. Instantaneous perturbation velocity vector plots and pressure fluctuations for two different phases within the blade passing cycle. Blue and red contours represent minimum and maximum of pressure fluctuations (i.e. mean subtracted), respectively.

shown in the iso-contours of the pressure fluctuations depicted in Fig. 3. The aft portion of the suction side is depicted in the 3D view of this picture for the two different phases shown in the previous plots. In the first phase the wake is not yet affecting the rear portion of the suction side, and a scarce population of coherent structures can be observed. Particularly, only small scale structures appear to be present over this portion of the blade at this phase. The cross-section on bottom of Fig. 3 helps the visualization of such structures (as observed by Michelassi *et al.* 2003), counter rotating vortical filaments that represent the leg of hairpin vortices are identified (similar to those observed also in Adrian 2007). In the second phase the flow shows the type of structures that are typically observed in turbulent flows, such as a train of hairpin vortices (that may be identified with a minimum of pressure as well as in the cross-stream plane) and boundary layer streaks. These structures are forced by the wake turbulence, as was already shown in Wu *et al.* (1999); Nagabhushana Rao *et al.* (2013); Coull & Hodson (2011); Lengani *et al.* (2016*a*), and are representative of the by-pass type transition process periodically induced by the passing wakes.

4.2. *POD analysis*

The instantaneous LES flow fields are highly complex, and a technique is required to rigorously identify the different dynamics responsible for loss generation. As a first step, POD is adopted in order to provide a statistical representation of the deterministic and stochastic contributions to the velocity fluctuations. The eigenvalues λ provide the kinetic energy captured by the POD modes, and give the first information of the relative importance of each mode. Figure 4 shows the POD eigenvalues normalized with the total

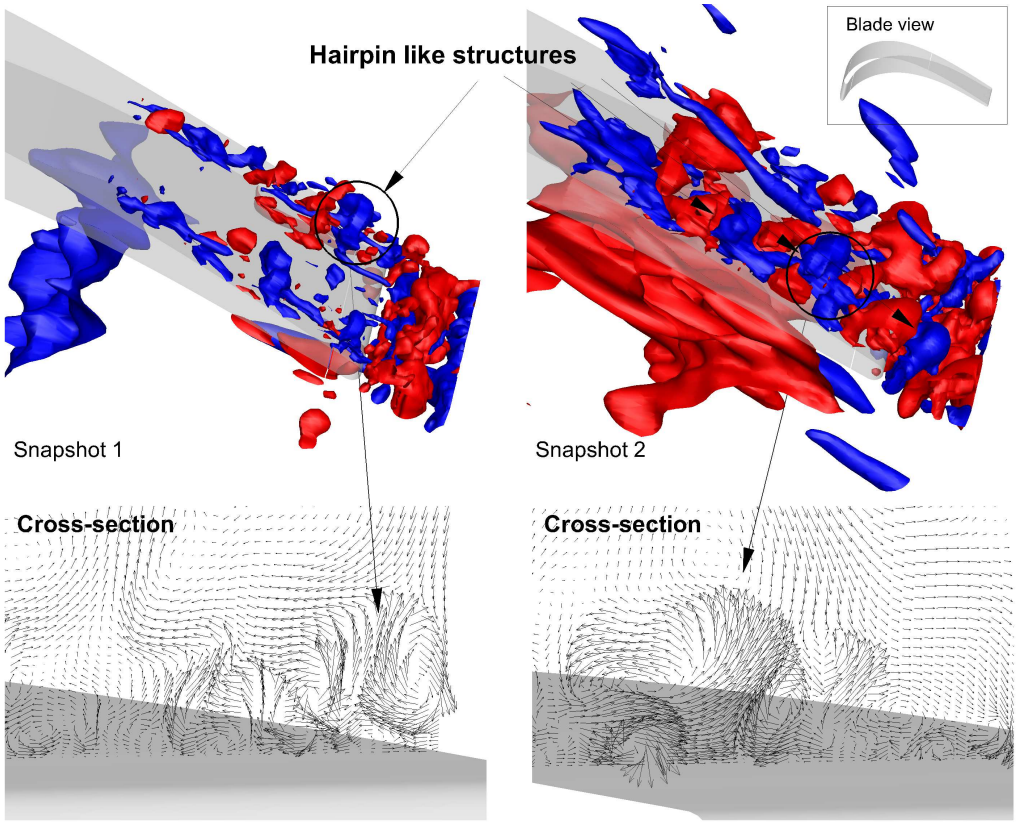

FIGURE 3. 3D view of the instantaneous pressure fluctuations for two different phases within the blade passing cycle. Blue and red iso-surfaces represent pressure fluctuations below and above a reference value, respectively.

kinetic energy. The first two modes have a total contribution of about 25% of the total energy, while the energy of the modes above the 100^{th} becomes lower than 0.1%. Even though the energy distribution seems rather similar for the modes above 3, the spatial distribution of the POD modes highlights different physical mechanisms involved in the generation of velocity fluctuations.

Some opportunely selected POD modes that exhibit different characteristics are shown in Fig. 5 as vectorial representations: each vector component is provided by the POD mode of the corresponding velocity component. The POD modes are orthonormal, thus the vector length for the different modes does not provide a direct comparison of their contribution to the velocity fluctuations. The isocontour plot represents the spatial distribution of the normalized TKE captured by the mode. This quantity is also represented in Fig. 6 that provides a 3D view of the rear part of the blade, where the isocontours with values close to the maximum levels are reported. It is used to highlight where the main flow features are identified, while to understand where losses are produced will be discussed in the next section.

The first two, most energetic, POD modes identify the large scale vortices that are associated with the deterministic "jet-like" structure induced by the wake (Sarkar & Voke 2006; Lengani *et al.* 2016*a*). Here, only the first mode is reported for the sake of brevity, since the second one basically depicts the same flow structures with the same energy content (see Fig.4) but spatially shifted. This behaviour is typical for pseudo-periodic

convective flows (Legrand *et al.* 2011*a*,*b*; Yarusevych & Kotsonis 2017; Wen *et al.* 2016). As discussed in a previous publication (Lengani *et al.* 2016*a*), these modes can be used to reconstruct the phase-averaged flow field and describe the migration of the traveling wake across the turbine passage, similarly to the generalized phase-averaged procedure described in (Bourgeois *et al.* 2013) to reconstruct the coherent motion behind a square cylinder. The structure represented by these first two modes divides into two branches; two counter-rotating vortices can clearly be identified in the pictures (highlighting the "negative-jet" like structure described in Stieger & Hodson 2004). Interestingly, the maximum TKE can be observed where the counter-clockwise rotating structures (the leading boundary of the wake) interact with the blade suction side, just behind the peak suction position. High values of TKE can also be observed close to the trailing edge. The 3D view of Fig. 6 shows evidence that these wake related modes are three-dimensional but they have a strong spanwise coherence.

Mode three is related to flow oscillations that occur in the rear part of the blade. The highest energy of these fluctuations is located on the blade pressure side, where typically Görtler vortices are present. It is authors' opinion that the low frequency motion of the streamwise vortex filament (as those observed in (Michelassi *et al.* 2003)) affecting the rear part of the blade pressure side is responsible for the quite large area traced by this mode. Indeed, it is worth noting that a single POD mode doeas not represent a structure, but more properly it provides a view of its best statistical representation. The fluctuating energy of this mode is particularly low within the blade passage and hence mode 3 seems to not be related to the upstream wake migration process. Furthermore, the 3D view of Fig. 6 makes clear that, conversely to mode 1 and mode 2, these fluctuations are related to 3-dimensional large scale structures which are oriented in the streamwise direction. The other modes depicted in the figures (modes 6 and 7) are again related to wake passing events, since they show coherent structures in the LPT passage similar to modes 1 and 2, but they also exhibit significant TKE levels in the rear part of the blade suction side. They are likely to represent the unsteady interaction between the wake and the boundary layer. This interaction is three dimensional, as depicted in Fig. 6, and the modes provide a statistical representation of the streaky structures induced by the periodic by-pass type transition process previously observed in the instantaneous images. Hence, the wake passing over the blade and interacting with the boundary layers leads to the generation of 3D structures and regions with high and low velocities within the boundary layer.

In order to better distinguish between wake migration and boundary layer related modes, a Fourier analysis of the POD eigenvectors was conducted and the results are shown in Fig. 7. The first two modes are strongly related to the wake passing frequency, identifiable as a sharp peak in the spectrum at wake passing frequency one. The modes related to Görtler vortices (modes 3 to 5) have high amplitude at low frequencies and, interestingly, a negligible contribution at the wake passing frequency and its higher harmonics. Conversely, the following modes, such as the 7^{th}, are again related to the wake passing frequency since they clearly exhibit higher harmonics of the fundamental frequency. Modes above 12 are no more related to the wake passing frequency or to the low frequency events. Results presented in this section make clearly evident that POD modes defined by the kinematic kernel are able to identify and split the different dynamics (i.e. related to wake or boundary layer) affecting the unsteady flow field characterizing the LPT passage. Moreover, by analyzing the POD mode distributions jointly with the spectral content presented here, it is also possible to associate families of modes with particular dynamics (i.e. related to the passing wake or not).

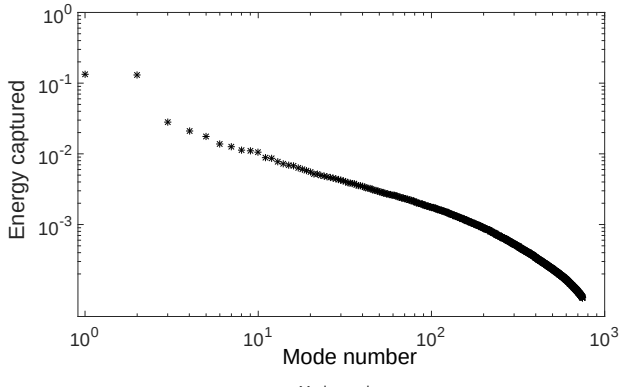

FIGURE 4. POD eigenvalues.

4.3. *TKE production*

As described in the previous sections the overall entropy rate of change (Eq. 3.4) is comprised of the sum of the effects related to TKE production, heat dissipated by the resolved scales, velocity-enthalpy correlation and viscous dissipation due to mean flow distortion. The fourth term, as previously discussed, cannot be decomposed per mode and is consequently not further considered in the present work. In the current work, the first three terms are analyzed separately, focusing on the contributions due to the different POD modes. Particularly, the TKE production, that is the main contribution to the loss generation is analyzed in details in this section, while the other two terms will be discussed in the next section.

The TKE production rate is shown in Figs. 8 as a 2D representation and in Fig. 9 as a 3D view on the rear part of the blade suction side. The first POD mode (and similarly the second one) generates the greatest amount of TKE inside the blade passage. The TKE production associated with this POD mode shows areas of positive and negative generation rate at the edges of the two large scale vortices generated in the passage during the wake migration. This mode clearly identifies zones where the turbulence is converted back to mean flow energy (red regions in the plot). This is similar to what occur in a 2D inviscid flow, there the flux of energy from large to small scales must be accompanied by another compensating flux of energy back toward larger length scales (**?**). In the present case, back-scatter occurs only locally, since once integrated over the whole domain (as done in the next section) the energy flux is from the mean flow to the turbulence. This mechanism of TKE production is almost uniform in the spanwise direction as highlighted by the 3D view of Fig. 9. The following modes show that TKE is produced mainly in the rear part of the blade in the boundary layer regions. Effects of mode 3 are prevalently confined in the pressure side region, while modes 6 and 7 exhibit marked TKE production in the rear part of the blade suction side. For these modes the production of TKE occurs by means of 3D structures elongated in the streamwise direction along the blade surface. Also in this case local back-scatter can be observed in between the elongated structures responsible for TKE production.

4.4. *Contribution to losses*

Since a single POD mode is not able to completely trace a "structure" or particular dynamics, the sum of the different terms (I, II and III) of eq. 3.4 for different ensembles of POD modes (i.e. a family pertaining/describing the same dynamics) is suited for the

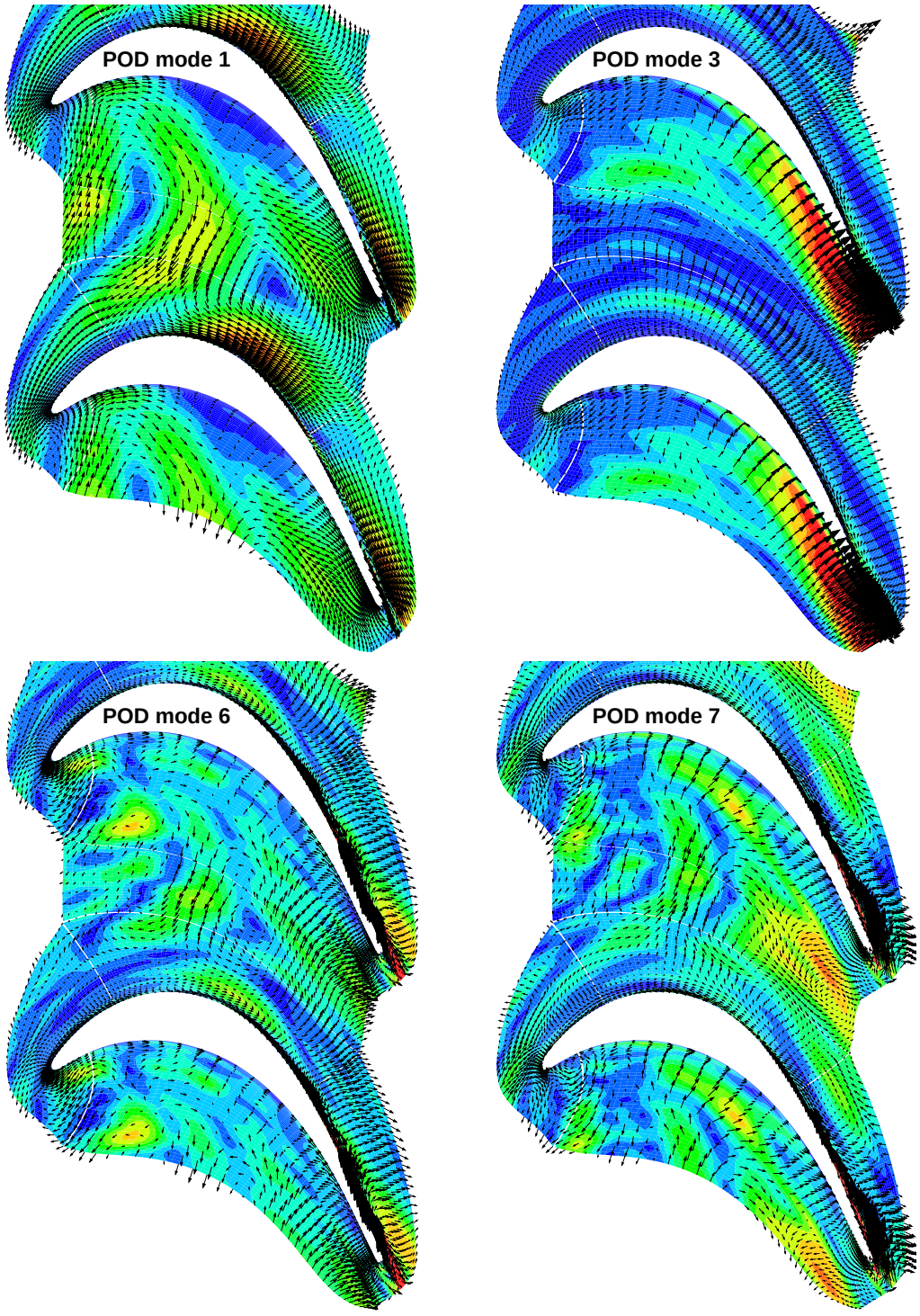

FIGURE 5. Vectorial representation of POD modes and spatial distribution of the TKE captured by the mode.

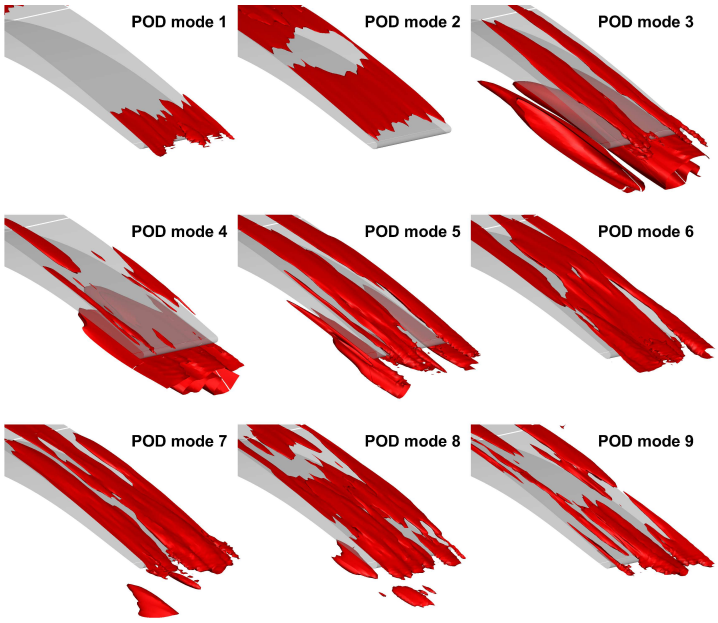

FIGURE 6. Isosurface of the TKE captured by the POD modes.

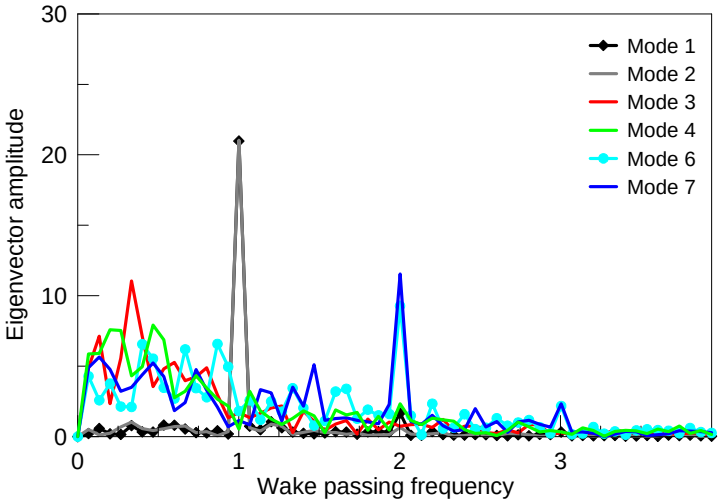

FIGURE 7. Spectral analysis of the POD eigenvectors.

identification of the contributions to entropy rate of change due to a particular dynamics. Once identified and isolated, the different POD families responsible for entropy rate of change, spatial integration in the whole 3D cascade passage provides, according to Eq. 3.4, the contribution of the different dynamics to the overall losses. The cumulative integral of the terms appearing in this equation is provided in Fig. 10. The cumulative contribution of the kinetic energy is also shown in the plot for comparison. The gray line provides the overall entropy rate of change in the full 3D domain, the labels of the axis (on the right) start from the base level of 40% that corresponds to the integral of the viscous dissipation (term IV of eq. 3.4). The red line represents the cumulative contribution of the TKE production. This is evidently the dominant term when compared with

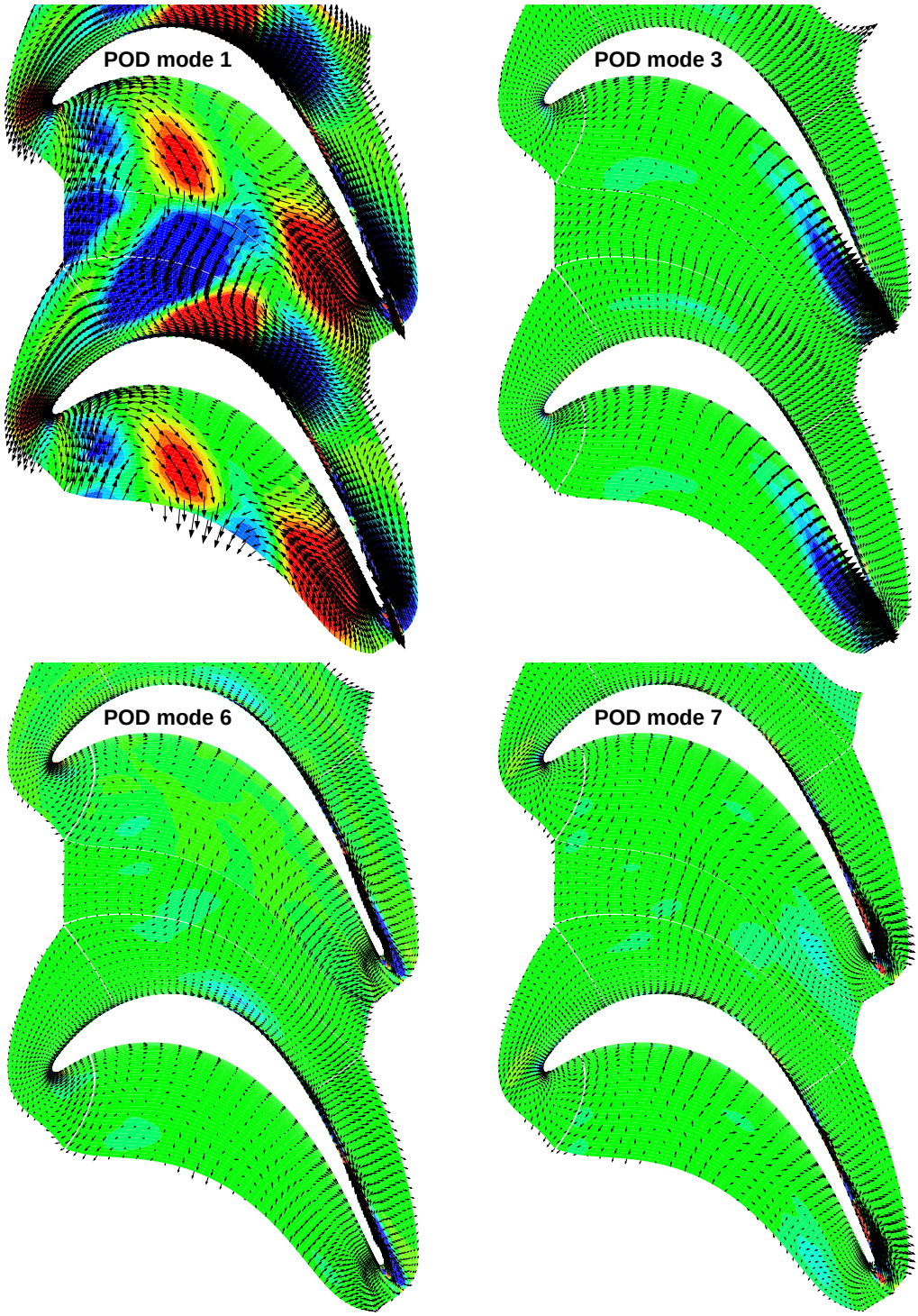

FIGURE 8. TKE production rate per POD mode.

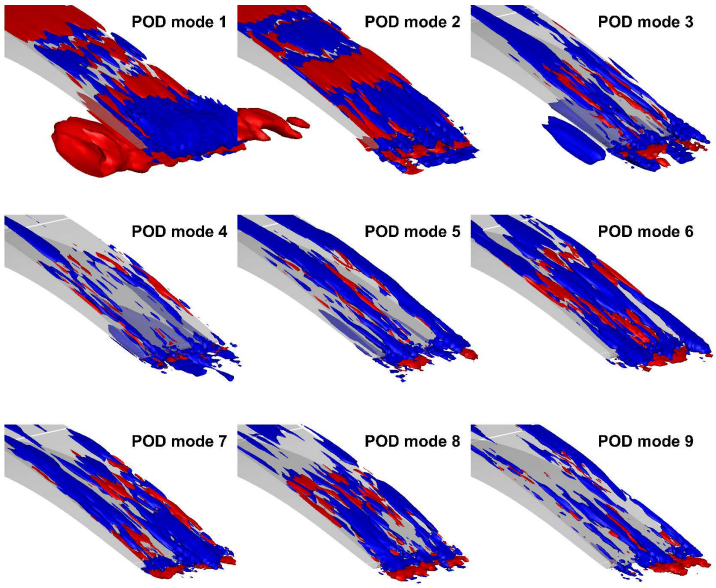

FIGURE 9. Isosurface of the TKE production rate per POD mode.

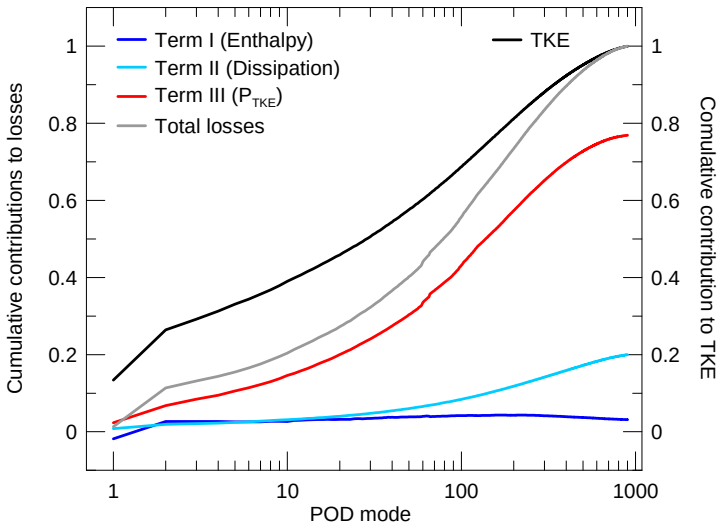

FIGURE 10. Cumulative contribution to the loss generation rate of each POD mode. The values are obtained by integration over the 3D measurement domain. The legend refers to Eq. 3.4

the other source terms. The dissipation term (light blue line) and the velocity-enthalpy correlation cover only slightly above 10% of the overall loss budget.

Looking at the different dynamics, the first 12 modes (excluding modes 3 to 5 as previously observed) describe the large scale structures carried by wake during migration, as identified from the Fourier analysis of their eigenvectors previously shown. The entropy rate of change related to these modes is about 12% of the total, while they capture about 35% of the TKE. It has to be noted that the contribution of the velocity-enthalpy correlation term is limited to the first two modes. The overall contribution due to velocity-enthalpy correlation is, in fact, determined by the fractions provided by summation of modes 1 and 2. This has the important consequence that reduced order models aimed at

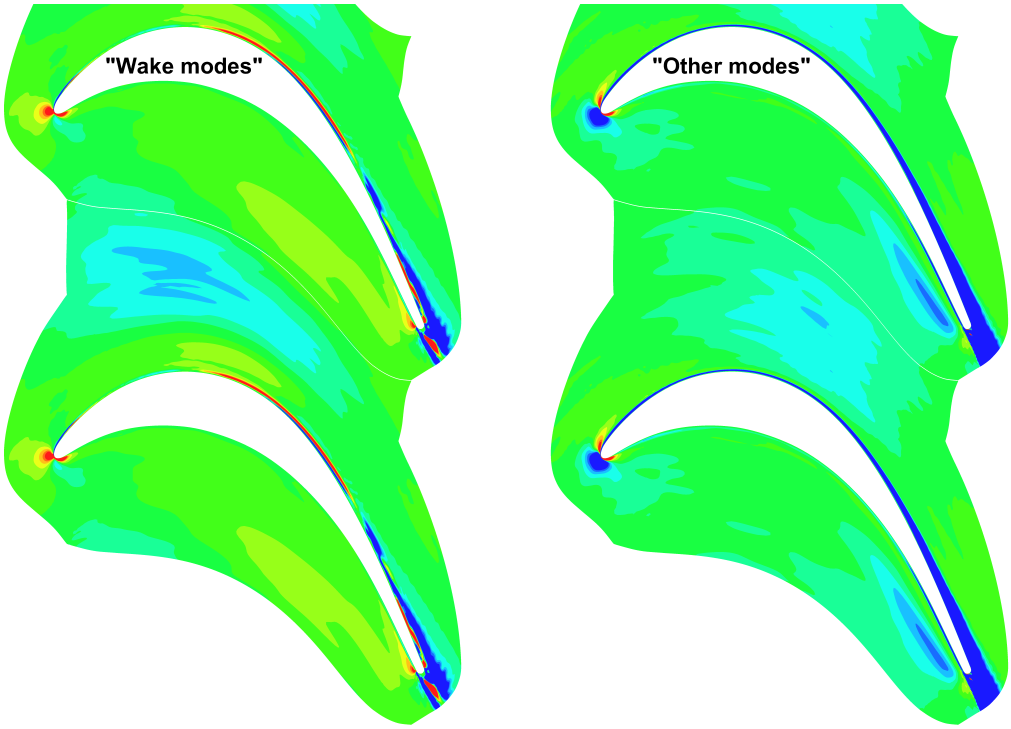

FIGURE 11. Entropy rate of change associated to the term III of eq. 3.4.

describing the effects due to velocity-enthalpy correlation can be constructed retaining (in the energy equation) just two POD modes (i.e. a Galerkin projection with only 2 modes provides almost 100% of the overall dynamics of the system). The dissipation term is significant only for the higher order POD modes (it becomes significant only after mode 20), according to what shown in Lengani *et al.* (2016*b*). In fact, the POD modes related to the large scale deterministic oscillations due to passing wake contribute marginally to the energy dissipation, due to the combination of viscosity and spatial derivative of the modes. Thus, a first important aspect raised by the present analysis is that losses due to the upstream wake propagation are essentially due to turbulence consumption, with negligible viscous dissipation. Consequently, wake migration related losses are expected to not be influenced by the variation of the Reynolds number.

In order to further empathize the capability of the procedure here proposed, the spatial distribution of the rate of change of entropy due to turbulent kinetic energy production and finer scales viscous dissipation (terms II and III of Eq. 3.4) are reported in Fig. 11 and 12, separating the loss contribution of the dynamics related to the wake propagation (modes from 1 to 10 excluded 3-5) and the rest (all the other modes). The 2D view only is proposed. Fig. 11 shows that the loss generation due to the large scale structures of the wake (plot on left) occurs within the passage (cyan region in the plot), as well as in the rear part of the suction side. The region of loss generation in the fore part of the potential flow region of the blade passage is observed where the phenomena of stretching and bowing of the wake are more pronounced. The loss production within the boundary layer observed behind the peak suction is instead related to interaction of the large scale structures of the wake and the decelerating boundary layer. The highest values can be observed in the rear part of the blade suction side, where the intermittent by-pass like transition is forced by the migrating wake. The loss generation due to the remaining

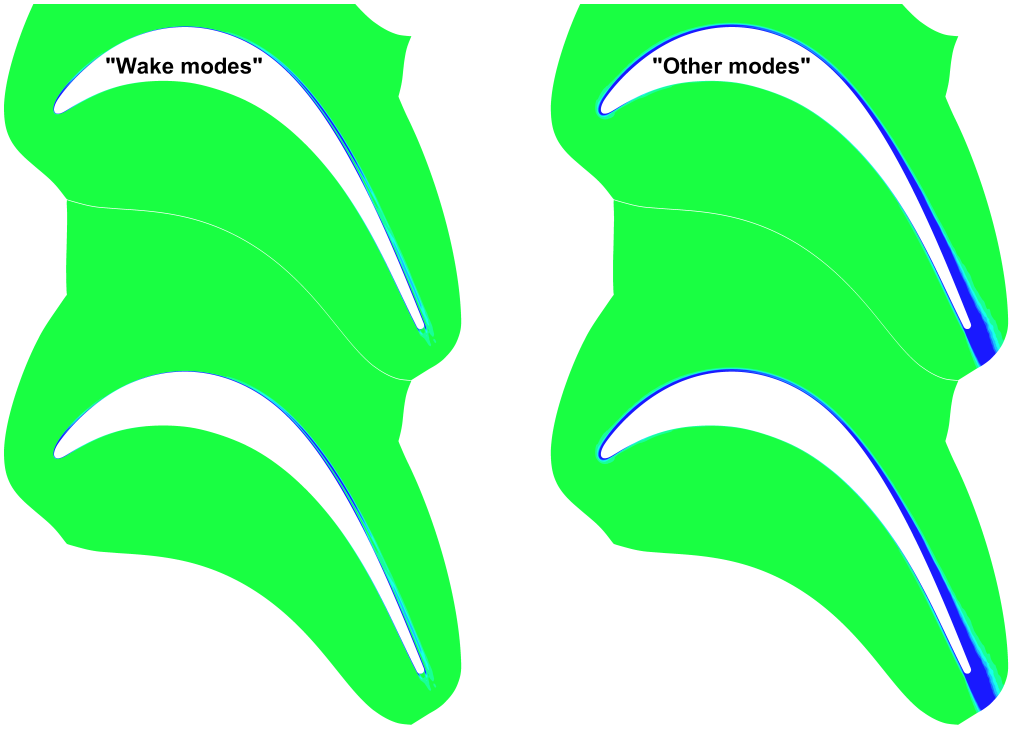

FIGURE 12. Entropy rate of change associated to the term II of eq. 3.4.

modes is mainly related to the boundary layer developing on the pressure and suction side since this mode family does not exibit any link to passing wake event (frequency). Particularly, the finer scale structures growing into the boundary layer (traced by the higher order, less energetic, POD modes) are responsible for the high level of entropy rate of change observable in the wall proximity on this plot in the rear suction and into the profile wake behind the trailing edge. Moreover, there is a not null contribution to the loss generation in the blade passage due to the higher order modes. This contribution is caused by the finer structures carried by the passing wakes during migration. In fact, the turbulence carried by the wake, that has a stochastic nature, is captured just by the higher order POD modes.

Fig. 12 shows the resolved scale dissipation (term II of Eq.3.4). This term is confined to the close to the wall region for both large scale wake related modes and the finer structures. This term is very small for the large scale wake related modes. It is mainly due to the finer structures generating during the wake-boundary layer interaction along the blade suction side. The contribution of this term in the potential flow region of the passage is negligible also for the remaining modes (plot on the right). This provides further evidence that energy dissipation due to the deterministic wake migration process is essentially due to the turbulence consumption, since viscous effects are negligible outside the boundary layer.

Finally, an analysis is performed to discriminate where (spatially) the same dynamics (i.e. POD family) acts to produce the largest amount of losses. To this end, spatial integration of the entropy rate of change has been limited to different flow regions: the boundary layer region, the potential flow region of the blade passage, and the mixing region downstream of the trailing edge. The former has been defined by a thresold level on the vorticity. The mixing region has been bounded by lines normal to the flow di-

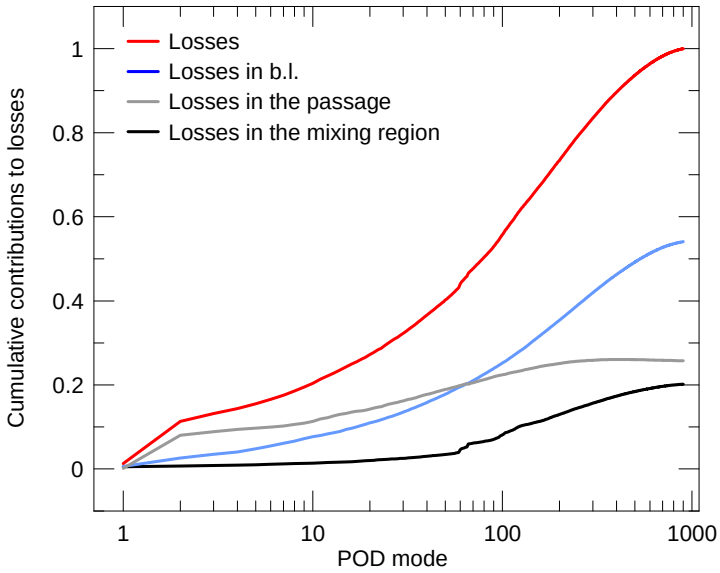

FIGURE 13. Cumulative contribution to the loss generation rate of each POD mode. The values are obtained by integration over the 3D measurement domain.

rection at the blade trailing edge, while the remaining space of the passage represent the potential flow region. Fig.XX provides a sketch of the different integration area. The results are shown in Fig. 13 in function of the POD modes. This is a quantitative plot to discuss what observed from the spatial distributions of previous plots. In fact, the losses obtained in the boundary layer region due to the large scale wake related POD modes give a direct estimation of the unsteady wake-boundary layer interaction process. On the other hand, losses due to the same family plus the finer scale dissipation restricted to the potential flow region isolates only the wake migrating losses.

The losses in the blade passage are about 15% of the total losses, and the modes related to the large scale structures of the wake contribute about 6% of the total losses there, the rest has to be attributed to higher POD modes. Thus, losses due to the finer structures embedded within the bulk of the wake (that have no significant amplitudes in the spectra) further contribute to the overall loss produced into the LPT passage during wake migration. It is suggested that the turbulence consumption terms (not viscous related) are probably linked to the energy cascade of turbulence. The large scale wake related modes partially contribute to the generation of TKE in the boundary layer (light blue line), but this contribution is only about 6% of the total. The remainder of the losses generated within the boundary layer are due to smaller scale structures (higher order POD modes); they represent about 25% of the total losses. The remaining 12% of the loss budget is generated in the mixing region, just downstream of the blade trailing edge. The first 50 modes do not contribute to the generation of losses in this region. Finally, modes 60 to 70, that identify the dynamics related to von Karman-type vortices (as shown by visual inspection of these modes, no shown for brevity), generate about 3% of total losses, while the remaining contribution is due to the finer scale structures caused by the mixing process in the profile wake.

5. Conclusions

The study of large datasets, such as time resolved LES of unsteady flow fields, requires large efforts in their interpretation. In the present paper, POD has been applied to high fidelity LES data of a low pressure turbine blade perturbed by unsteady passing wakes in order to characterize and split the different phenomena and dynamics responsible for loss generation. The procedure takes care of the bi-orthogonality condition of POD modes and related temporal coefficients to evaluate the entropy rate of change related to each POD mode, thus allowing the identification of effects due to incoming wake migration, boundary layer events and coherent structures originated by the wake-boundary layer interaction process.

The procedure has been shown to be clearly able in identifying the different phenomena generating the complex unsteady flow field, namely: the large scale structures attached to the leading and trailing boundaries of the wake as well as the smaller streamwise oriented scale generating into the boundary layer as a consequence of the by-pass like transition process induced by wakes. Particularly, the effect of the large scale structures attached to the wake is very well captured by the first, most energetic, POD modes that constitute an optimal, in statistical terms, representation of the flow field. Higher order POD modes trace instead streaky structures. It has been shown that the Fourier transform of the temporal eigenvector allow the association between modes and the deterministic events related (or not) to the periodic passing wakes.

The different terms that contribute to the entropy rate of change have been evaluated separately, projecting the velocity and enthalpy fields onto the orthogonal basis spanned by the temporal coefficient obtained by the kinematic kernel. The production of turbulent kinetic energy is the term that contribute the most. The largest values are observed within the blade passage and in the boundary layers. The first modes capture the loss increase due to the large scale structures of the wake migrating into the potential flow region, and highlight that it occurs mainly in the fore part of the blade passage where the two large scale structures of the wake are dilated, stretched and bowed. Regions of back-scatter are also observed, locally the turbulence may be converted back to mean flow energy. However, the energy flux per POD mode, once integrated over the volume, is from the mean flow to the turbulence. The dissipation term and velocity-enthalpy correlation cover only slightly above 20% of the overall loss budget. The dissipation occur just within the boundary layer, with negligible contribution due to the large scale structure carried by the wake both in the potential and in the boundary layer region. On the other hand, the velocity-enthalpy correlation term is capture in its entirety by just the first two POD modes.

The entropy rate of change has been evaluated over the whole domain as well as in properly defined control volumes. In the present case, the boundary layer, the blade passage, and the blade wake regions have been chosen as integration volumes to provide a split of the loss source not presented before. The cumulative contribution of the losses for each POD mode and for the specified region allows a very fast evaluation of where the loss come from, and by which dynamical feature they are caused. Hence, the loss contribution from a large dataset of a complex 3D unsteady flow field may be easily extracted using the proposed post-processing procedure in other applications described either by numerical or experimental data.

REFERENCES

Adrian, R. J. 2007 Hairpin vortex organization in wall turbulence. *Phys. Fluids* **19**, 041301–1–041301–16.

Alam, M. & Sandham, N. 2000 Direct numerical simulation of 'short' laminar separation bubbles with turbulent reattachment. *J. Fluid Mech.* **410**, 1–28.

Binder, A., Förster, W., Kruse, H. & Rogge, H. 1985 Experimental investigation into the effect of wakes on the unsteady turbine rotor flow. *ASME Journal of Engineering for Gas Turbines and Power* **107** (2), 458–465.

Binder, A., Schröder, Th. & Hourmouziadis, J. 1989 Turbulence measurements in a multistage low-pressure turbine. *J Turbomach* **111** (2), 153–161.

Borée, J 2003 Extended proper orthogonal decomposition: a tool to analyse correlated events in turbulent flows. *Experiments in fluids* **35** (2), 188–192.

Bourgeois, JA, Noack, BR & Martinuzzi, RJ 2013 Generalized phase average with applications to sensor-based flow estimation of the wall-mounted square cylinder wake. *Journal of Fluid Mechanics* **736**, 316–350.

Coull, J. D. & Hodson, H. P. 2011 Unsteady boundary-layer transition in low-pressure turbines. *J. Fluid Mech.* **681**, 370–410.

Denton, J Do 1993 Loss mechanisms in turbomachines. In *ASME 1993 International Gas Turbine and Aeroengine Congress and Exposition*, pp. V002T14A001–V002T14A001. American Society of Mechanical Engineers.

Hodson, Howard P & Howell, Robert J 2005 Bladerow interactions, transition, and high-lift aerofoils in low-pressure turbines. *Annu. Rev. Fluid Mech.* **37**, 71–98.

Hussain, A. & Reynolds, W. 1970 The mechanics of an organized wave in turbulent shear flow. *J. Fluid Mech.* **41**, 241–258.

Jones, L., Sandberg, R. & Sandham, N. 2008 Direct numerical simulations of forced and unforced separation bubbles on an airfoil at incidence. *J. Fluid Mech.* **602**, 175–207.

Kurelek, John W, Lambert, Andrew R & Yarusevych, Serhiy 2016 Coherent structures in the transition process of a laminar separation bubble. *AIAA Journal* pp. 1–15.

Legrand, M., Nogueira, J. & Lecuona, A. 2011*a* Flow temporal reconstruction from non-time-resolved data part I: mathematic fundamentals. *Exp. Fluids* **51** (4), 1047–1055.

Legrand, M., Nogueira, J., Tachibana, S., Lecuona, A. & Nauri, S. 2011*b* Flow temporal reconstruction from non-time-resolved data part II: practical implementation, methodology validation, and applications. *Exp. Fluids* **51** (4), 861–870.

Lengani, Davide, Simoni, Daniele, Ubaldi, Marina, Zunino, Pietro & Bertini, Francesco 2016*a* Coherent structures formation during wake-boundary layer interaction on a lp turbine blade. *Flow, Turbulence and Combustion* pp. 1–25.

Lengani, Davide, Simoni, Daniele, Ubaldi, Marina, Zunino, Pietro & Guida, Roberto 2016*b* Turbulence production, dissipation and length scales in laminar separation bubbles. *ETMM11* pp. 1–6.

Liu, Z., Adrian, Ro Jo & Hanratty, To Jo 2001 Large-scale modes of turbulent channel flow: transport and structure. *J. Fluid Mech.* **448**, 53–80.

Lumley, J. L. 1967 The structure of inhomogeneous turbulent flows. *A.M. Yaglom, V.I. Tatarski (Eds.), Atmospheric Turbulence and Wave Propagation* pp. 166–178.

Michelassi, Vittorio, Chen, Liwei, Pichler, Richard, Sandberg, Richard & Bhaskaran, Rathakrishnan 2016 High-fidelity simulations of low-pressure turbines: Effect of flow coefficient and reduced frequency on losses. *Journal of Turbomachinery* **138** (11), 111006.

Michelassi, Vittorio, Chen, Li-Wei, Pichler, Richard & Sandberg, Richard D 2015 Compressible direct numerical simulation of low-pressure turbines-part II: Effect of inflow disturbances. *Journal of Turbomachinery* **137** (7), 071005 1–12.

Michelassi, V, Wissink, JG, Fr-Ograve, J, hlich & Rodi, W 2003 Large-eddy simulation of flow around low-pressure turbine blade with incoming wakes. *AIAA journal* **41** (11), 2143–2156.

Michelassi, Vittorio & Wissink, Jan G 2015 Turbulent kinetic energy production in the vane of a low-pressure linear turbine cascade with incoming wakes. *International Journal of Rotating Machinery* **2015**.

Nagabhushana Rao, V, Tucker, PG, Jefferson-Loveday, RJ & Coull, JD 2013 Large eddy simulations in low-pressure turbines: Effect of wakes at elevated free-stream turbulence. *Int. J. Heat Fluid Flow* **43**, 85–95.

Perrin, R., Cid, E., Cazin, S., Sevrain, A., Braza, M., Moradei, F. & Harran, G. 2007

Phase-averaged measurements of the turbulence properties in the near wake of a circular cylinder at high reynolds number by 2C-PIV and 3C-PIV. *Exp Fluids* **42**, 93–109.

Praisner, TJ, Clark, JP, Nash, TC, Rice, MJ & Grover, EA 2006 Performance impacts due to wake mixing in axial-flow turbomachinery. In *ASME Turbo Expo 2006: Power for Land, Sea, and Air*, pp. 1821–1830.

Rogers, Michael M 2002 The evolution of strained turbulent plane wakes. *Journal of Fluid Mechanics* **463**, 53–120.

Sarkar, S. 2008 Identification of flow structures on a LP turbine blade due to periodic passing wakes. *J. Fluid Eng - T ASME* **130**, 061103 (10 pages).

Sarkar, S. & Voke, P. 2006 Large-eddy simulation of unsteady surface pressure overa low-pressure turbine blade due to interactions of passing wakes and inflexional boundary layer. *ASME J. of Turbomach.* **128**, 221–231.

Satta, Fo, Simoni, Do, Ubaldi, Mo, Zunino, Po & Bertini, Fo 2014 Loading distribution effects on separated flow transition of ultra-high-lift turbine blades. *AIAA J. of Prop. and Power* **30**, 845–856.

Simoni, D., Ubaldi, M. & Zunino, P. 2013 Experimental investigation of the interaction between incoming wakes and instability mechanisms in a laminar separation bubble. *Exp. Therm. Fluid Sci* **50**, 54–60.

Sirovich, L. 1987 Turbulence and the dynamics of coherent structures. part I-III. *Q Appl Math* **45**, 561–590.

Stieger, R. D. & Hodson, H. 2004 The transition mechanism of highly loaded low-pressure turbine blades. *ASME J. of Turbomach.* **126**, 536–543.

Stieger, R. D. & Hodson, H. P. 2005 The unsteady development of a turbulent wake through a downstream low-pressure turbine blade passage. *ASME J. of Turbomach.* **127**, 388–394.

van Oudheusden, B. W., Scarano, F., van Hinsberg, N. P. & Watt, D. W. 2005 Phase-resolved characterization of vortex shedding in the near wake of a square-section cylinder at incidence. *Exp. Fluids* **39**, 86–98.

van de Wall, Allan G, Kadambi, Jaikrishnan R & Adamczyk, John J 2000 A transport model for the deterministic stresses associated with turbomachinery blade row interactions pp. V001T03A006–V001T03A006.

Wen, Xin, Tang, Hui & Duan, Fei 2016 Interaction of in-line twin synthetic jets with a separated flow. *Physics of Fluids* **28** (4), 043602.

Wu, X., Jacobs, R.G., Hunt, J. C. R. & Durbin, P. A. 2001 Evidence of longitudinal vortices evolved from distorted wakes in a turbine passage. *J. Fluid Mech.* **446**, 199–228.

Wu, Xiaohua, Jacobs, Robert G, Hunt, Julian CR & Durbin, Paul A 1999 Simulation of boundary layer transition induced by periodically passing wakes. *Journal of Fluid Mechanics* **398**, 109–153.

Yarusevych, Serhiy & Kotsonis, Marios 2017 Effect of local dbd plasma actuation on transition in a laminar separation bubble. *Flow, Turbulence and Combustion* **98** (1), 195–216.

Zaki, TA, Wissink, JG, Durbin, PA & Rodi, W 2009 Direct computations of boundary layers distorted by migrating wakes in a linear compressor cascade. *Flow, turbulence and combustion* **83** (3), 307–322.